Energetic Features of H-bonded and π-stacked Assemblies in Pyrazole-based Coordination Compounds of Mn(II) and Cu(II): Experimental and Theoretical Studies

Mridul Boro , Trishnajyoti Baishya , Antonio Frontera * , Miquel Barceló-Oliver , Manjit K Battacharyya *

Posted Date: 11 March 2024

doi: 10.20944/preprints202403.0550.v1

Keywords: Mononuclear Coordination Compound; Aromatic π-stacking; DFT; QTAIM; NCI

Article

Energetic Features of H-Bonded and π-Stacked Assemblies in Pyrazole-Based Coordination Compounds of Mn(II) and Cu(II): Experimental and Theoretical Studies

Mridul Boro [a], Trishnajyoti Baishya [a], Antonio Frontera [b,*], Miquel Barceló-Oliver [b] and Manjit K. Bhattacharyya [a,*]

[a] Department of Chemistry, Cotton University, Guwahati-781001, Assam, India
[b] Departament de Química, Universitat de les Illes Balears, Crta de Valldemossa km 7.7, 07122 Palma de Mallorca (Baleares), Spain
* Correspondence: toni.frontera@uib.es (A.F.); manjit.bhattacharyya@cottonuniversity.ac.in (M.K.B.)

Abstract: Two new coordination compounds of Mn(II) and Cu(II) *viz*. $[Mn(bz)_2(Hdmpz)_2(H_2O)]$ (**1**) and $[Cu(crot)_2(Hdmpz)_2]$ (**2**) (where, bz = benzoate, crot = crotonate, Hdmpz = 3, 5-dimethyl pyrazole) have been synthesized and characterized using single crystal X-ray diffraction technique, FT-IR, electronic spectroscopy, TGA and elemental analyses. Compounds **1** and **2** crystallize as mononuclear coordination compounds of *Hdmpz* based penta-coordinated Mn(II) and hexa-coordinated Cu(II) respectively containing distorted trigonal bipyramidal and distorted octahedral geometries. Crystal structure analysis of compound **1** reveals the presence C–H···π and π-stacking interactions along with O–H···O, N–H···O and C–H···O H-bonding interactions which stabilizes the layered assembly of the compound. Similarly, the presence of hydrogen bonding along with π-stacking interactions stabilizes the crystal structure of compound **2**. We have carried out theoretical investigations to analyze π···π H-bonding and antiparallel CH···π non-covalent interactions observed in the compounds. DFT calculations were performed to evaluate strength of these interactions energetically. Moreover, QTAIM and non-covalent interaction (NCI) plot index computational tool were used to characterize them and evaluate the contribution of the H-bonds.

Keywords: mononuclear coordination compound; aromatic π-stacking; DFT; QTAIM; NCI

1. Introduction

There has been significant interest of mixed ligand metal-organic frameworks in the field of supramolecular chemistry owing to their wide potential applications in magnetic devices, non-linear optics, catalysis, sorption, electrical conductivity, sensors and biology [1–7]. But the synthesis and development of single crystals of desired architectures and prospective demands is still challenging as the self-assembled processes is highly dependent on various experimental factors *viz*. coordination environment of the central metal ion, nature of the ligands used, metal to ligand ratio, reaction environments etc [8–12]. Appropriate fusion of these synthetic parameters is very important to achieve desired supramolecular architecture having potential use [13].

The interpretation of the non-covalent interactions is the backbone of self-assembled architectures as they form the basis of highly specific recognition, transport and regulatory mechanisms [14–16]. The most substantial changes in the properties of the self-assembled molecules take place, as the way in which non-covalent interactions like aromatic π-stacking, C–H···π, and wide varieties of hydrogen bonding interactions operate. The directionality and cumulative strength of these non-covalent interactions provide an organizing force for association of the molecules into

 doi:10.20944/preprints202403.0550.v1

fascinating self-assembled structures [17–22]. In addition, non-covalent interactions play key roles in biological systems which involve drug-receptor interactions, protein folding etc [23–25]. Therefore, to investigate and quantify various non-covalent interactions observed in self-assembled architectures, countless efforts have been put in till date [26,27].

In recent times, N and O donor ligands elicit significant attention from chemists to design fascinating self-assembled architectures with various important uses [28,29]. Transition metal coordination complexes involving aliphatic and aromatic carboxylates provide versatile and interesting structural networks due to their ability to coonect through monodentate as well as bidentate coordination modes [30,31]. In a similar way, complexes involving pyrazole ligands, due to their diverse structural topologies, are efficient and versatile in various fields that includes medicine, catalysis, separations, bio-mimetic chemistry, optics, magnetism and luminescence etc. [32–35]. Pyrazole complexes with varied pharmacological actions, including antifungal [36,37], antibacterial [38] and anticancer properties, have also been reported due to their role in the development of newer drugs [39–42]. Moreover, the coordination chemistry of transition metal based drugs has gained interest because of their applications in cancer management [43–45]. Transition metals like manganese are involved in various important biological processes, from electron transfer to catalysis to structural roles and are associated with active sites of many proteins and enzymes [46]. In addition, the Mn(II) complexes exhibit interesting electrochemical, biological and magnetic properties [47,48]. The flexibility of the Cu(II) ion, due to its transition elemental nature, enhances its coordination preferences with aromatic and aliphatic ligands [49]. The crystal structures of copper complexes with mixed N- and O-donor ligands are reported in the literature [50,51]. Depending on the ligand binding sites, some Cu(II) complexes possess a wide range of biological activity, such as antibacterial, fungicidal, pesticidal and even as tracers [52,53].

In order to explore the interplay of non-covalent interactions in supramolecular architectures, two new Mn(II) and Cu(II) coordination compounds viz. $[Mn(bz)_2(Hdmpz)_2(H_2O)]$ (1) and $[Cu(crot)_2(Hdmpz)_2]$ (2) have been synthesized and characterized using single crystal X-ray diffraction technique, FT-IR, electronic spectroscopy, TGA and elemental analyses. Crystal structure analysis of compound 1 unfolds the presence of C–H···π and π-stacking interactions along with O–H ···O, N–H···O and C–H···O H-bonding interactions which stabilizes the layered assembly of the compound. Aromatic π-stacking interactions, C–H···O, N–H···O hydrogen bonds along with non-covalent C–H···C interactions stabilizes the crystal structure of compound 2. We have carried out theoretical investigations to analyze π-stacking, H-bonds and C–H···π interactions observed in compounds 1 and 2. The interactions have been characterized by using the quantum theory of atoms-in-molecules (QTAIM) and the non-covalent interaction (NCI) plot index computational tools.

2. Experimental Section

2.1. Materials and methods

All the chemicals viz. manganese (II) chloride tetrahydrate, copper(II) chloride dihydrate, benzoic acid, 3,5-dimethyl pyrazole and crotonic acid used in this work were purchased from commercial sources and used without further purification. Elemental analyses of the compounds were carried out using Perkin Elmer 2400 series II CHN analyzer. FT-IR spectra (KBr phase) of the compounds were recorded using Bruker Alpha (II) Infrared spectrophotometer in the frequency range of 4000-500 cm^{-1}.Shimadzu UV-2600 spectrophotometer was used to record the electronic spectra of the compounds. $BaSO_4$ powder was used as reference (100% reflectance) to record the solid state spectra. Room temperature magnetic moments of the compounds were calculated at 300 K on Sherwood Mark 1 Magnetic Susceptibility balance by Evans method. Thermogravimetric curves of the compounds were obtained under the flow of N_2 gas using Mettler Toledo TGA/DSC1 STAR^e system at the heating rate of $10^oC\ min^{-1}$.

2.2. Synthesis

 doi:10.20944/preprints202403.0550.v1

2.2.1. Synthesis of $[Mn(bz)_2(Hdmpz)_2(H_2O)]$ (1)

A mixture of $MnCl_2{\cdot}4H_2O$ (0.197 g, 1 mmol) and sodium salt of benzoic acid (0.288 g, 2 mmol) was dissolved in 10 mL of de-ionized water in a round bottomed flask and mechanically stirred at room temperature for two hours. To the resulting solution; Hdmpz (0.192g, 2 mmol) was added slowly and kept stirring for another hour (Scheme 1). The resulting solution was then kept unperturbed in cooling conditions (2-4°C) for crystallization. After several days, yellow coloured block shaped single crystals suitable for single crystal X-ray diffraction was obtained. Yield: 0.465 g (92.26%). Anal. calcd. for $C_{24}H_{28}MnN_4O_5$ C, 56.81%; H, 5.56%; N, 11.04%; Found: C, 54.64%;H, 5.47%; N, 10.99%. FT-IR (KBr pellet, cm^{-1}): 3439(br), 3130(w),2837 (m), 1593(s), 1429(m), 1389(s), 1280(m), 1145 (m), 1108(w), 975(w), 772(m), 715(m), 655(s) (s, strong; m, medium; w, weak; br, broad; sh, shoulder).

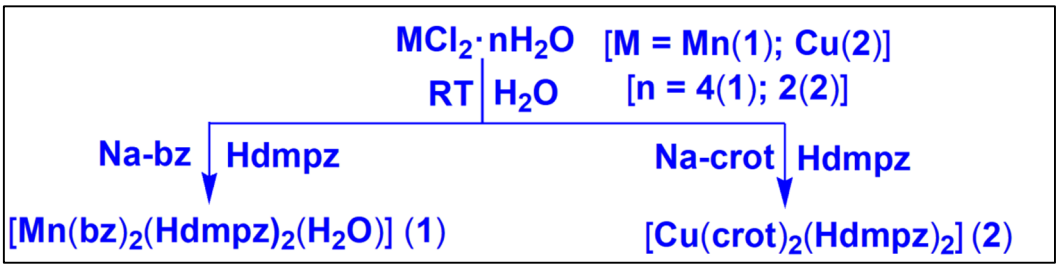

Scheme 1. Synthesis of the compounds **1** and **2**.

2.2.2. Synthesis of $[Cu(crot)_2(Hdmpz)_2]$ (2)

$CuCl_2{\cdot}2H_2O$ (0.170 g, 1 mmol) and sodium salt of crotonic acid (0.210 g, 2 mmol) were mixed in 10 mL of de-ionized water in a round bottom flask and the solution was allowed to stir mechanically for about two hours. Hdmpz (0.192 g, 2 mmol) was then added to the resulting solution and kept for mechanical string for another hour (Scheme 1). Then, the resulting solution was kept undisturbed in a refrigerator (below 4°C) for crystallization. Blue block shaped single crystals were obtained by the slow evaporation of the mother liquor after several days. Yield: 0.386 g (90.82%). Anal. calcd. for $C_{18}H_{26}CuN_4O_4$: C, 50.75%; H, 6.15%; N, 13.15%; Found: C,50.67%; H, 6.09%; N, 13.09%. IR (KBr pellet, cm^{-1}): 3439(br), 3132(sh), 2845(m), 1593(s), 1430(m), 1414(s), 1288(m), 1150(m), 1115(w), 1045(m), 944(w), 849(m), 740(m), 670(m), 498(w) (s, strong; m, medium; w, weak; br, broad; sh, shoulder).

2.3. Crystallographic data collection and refinement

Molecular and crystal structures of the compounds were determined using single crystal X-ray diffraction technique. X-ray diffraction data collection was carried out using Bruker APEX-II CCD diffractometer with graphite mono-chromatized Cu/Kα radiation (λ = 1.54178 Å). Semi-empirical absorption correction, as well as scaling and merging of the different datasets for the wavelength were performed using SADABS [54]. Crystal structures were solved by direct method and refined using full matrix least squares technique with SHELXL-2018/ [55] using the using the WinGX [56] software. All the non-hydrogen atoms were refined anisotropically. The hydrogen atoms except those attached to the O-atoms of water molecules were placed at their calculated positions and refined in the isotropic approximation. The hydrogen atoms of the coordinated water molecules are fixed at the nominal X-ray distances from the O-atoms to obtain the hydrogen bonding patterns in the crystal structures. Diamond 3.2 [57] software was used to draw the structural diagrams. Crystallographic data of the compounds **1** and **2** are tabulated in Table 1.

Table 1. Crystallographic data and structure refinement details for the compounds **1** and **2.**

Crystal Parametres	**1**	**2**
Emprical formula	$C_{24}H_{28}MnN_4O_5$	$C_{18}H_{26}CuN_4O_4$

 doi:10.20944/preprints202403.0550.v1

Formula weight	507.44	425.97
Temperature (K)	100.0	100.0
Wavelength (Å)	1.54178	1.54178
Crystal system	Orthorhombic	Orthorhombic
Space group	Pbcn	Pbcn
a/Å	19.2401 (1)	15.6899(5)
b/Å	12.1579(7)	10.7161(3)
c/Å	10.1312(6)	11.3062(4)
α º	90	90
βº	90	90
γ º	90	90
Volume (Å^3)	*2369.9(2)*	*1900.96(1)*
Z	4	4
Calculated density (g/cm^3)	1.422	1.488
Absorption coefficient (mm^{-1})	4.893	1.897
F(000)	1060	892
Crystal size (mm^3)	0.35×0.21×0.18	0.31×0.22×0.12
θ range for data collection(º)	10.76 to 136.33	1.604 to 23.973
Index ranges	-23<=h<=23, -14<=k<=14, -11<=l<=12	-18<=h<=18, -12<=k<=12, -13<=l<=13
Reflections collected	19422	28974
Unique data(R_{int})	2972	1721
Refinement method	Full-matrix least squares on F^2	Full-matrix least-squares on F^2
Data / restraints / parameters	2136/1/161	1721/0/126
Goodness-of-fit on F^2	1.086	1.143
Final *R*indices[$I>2\sigma(I)$] *R*1/ *w*R2	R1 = 0.0414, wR2 = ‘0.1110	R_1 = 0.0475, wR_2 = 0.1395
*R*indices(all data) *R*1/ *w*R2	R1 = 0.0434, wR2 = 0.1133	R_1 = 0.0482, wR_2 = 0.1402
Largest diff. peak and hole (e.Å^{-3})	0.45/-0.49	0.37/-0.63

2.4. Computational methods

Using the Gaussian-16 program [58] and the PBE0 [59]-D3 [60]/def2-TZVP [61] level of theory, the single point calculations were carried out. The crystallographic coordinates have been used to evaluate the interactions in the compounds since we are interested to study the non-covalent interactions standing in the solid state. The Bader's “Atoms in molecules” theory (QTAIM) [62] and non-covalent interaction plot (NCI Plot) [63] were used to study the interactions discussed herein using the AIMAll program [64]. To calculate the H-bond energies, we used the equation proposed by Espinosa et al (E = ½Vr) [65].

3. Results and discussion

3.1. Syntheses and general aspects

 doi:10.20944/preprints202403.0550.v1

$[Mn(bz)_2(Hdmpz)_2(H_2O)]$ (**1**) has been synthesized by the reaction between one equivalent of $MnCl_2{\cdot}4H_2O$, two equivalents of sodium salt of benzoic acid and two equivalents of Hdmpz at room temperature. Similarly, $[Cu(crot)_2(Hdmpz)_2]$ (**2**) has been prepared by reacting one equivalent of $CuCl_2{\cdot}2H_2O$, two equivalents of sodium salt of crotonic acid and two equivalents of Hdmpz at room temperature in de-ionized water medium. Both the compounds **1** and **2** are soluble in water and in common organic solvents. Compounds **1** and **2** show room temperature (298 K) μ_{eff} value of 5.89 and 1.82 BM respectively which suggests the presence of five and one unpaired electron(s) in the Mn(II) and Cu(II) centers of the distorted trigonal bipyramidal and distorted octahedral coordination spheres [66,67].

3.2. Crystal structure analysis

Figure 1 depicts the molecular structure of compound **1**. Compound **1** crystallizes in orthorhombic crystal system with Pbcn space group. Selected bond lengths and bond angles have been summarized in Table 2.

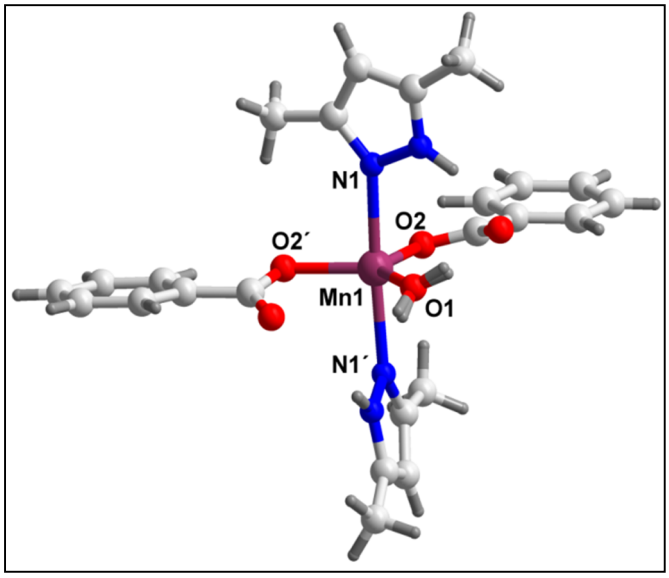

Figure 1. Molecular structure of $[Mn(bz)_2(Hdmpz)_2(H_2O)]$ (**1**).

In the compound, the Mn(II) metal centre is penta-coordinated to two monodentate bz moieties, two monodentate Hdmpz and one water molecule. The coordination geometry around the Mn1 centre in the compound is slightly distorted trigonal bipyramidal as evidenced by the trigonality index value (τ) of 0.77 [68], where the axial sites are occupied by N1 and N1′ atoms from Hdmpz moieties while the equatorial sites are occupied by O1, O2 and O2′ from coordinated water and bz moieties respectively. The bond lengths between the Mn1 and the nitrogen atoms of Hdmpz (N1 and N1′) are found to be 2.32(2) Å; whereas, that between the Mn1 and oxygen atoms of bz moieties (O2 and O2′) are 2.08(1) Å. The bond length between the Mn1 centre and the oxygen atom (O1) of the coordinated water molecule is found to be 2.13 Å. Crystal structure analysis reveals that hydrogen atoms (H1A and H1B) of the coordinated water molecule have the site occupancy factor of 0.5.

Table 2. Selected bond lengths (Å) and bond angles (°) around the Mn(II) centers in **1** and **2** respectively.

Bond lengths of **1** (Å)		Bond angles of **1** (°)	
Mn1–O2	2.0854(1)	O2–Mn1–O2′	106.18(8)
Mn1–O2′	2.0854(1)	O2–Mn1–O1	126.91(4)
Mn1–O1	2.132(2)	O2′–Mn1–O1	126.91(4)
Mn1–N1	2.3173(2)	O2–Mn1–N1′	92.39(5)

 doi:10.20944/preprints202403.0550.v1

Mn1–N1′	2.3173(2)	O2–Mn1–N1	91.72(6)
		O1–Mn1–N1	86.57(4)
		O1–Mn1–N1′	86.57(4)
		O2′–Mn1–N1′	91.72(6)
		O2′–Mn1–N1	92.40(5)
		N1–Mn1–N1′	173.15(8)

Bond lengths of **2** (Å)		Bond angles of **2** (°)	
Cu1–N1	1.989(3)	N1–Cu1–N1′	93.24(1)
Cu1–N1′	1.989(3)	N1–Cu1–O1	165.45(9)
Cu1–O1′	2.002(2)	N1–Cu1–O1′	91.47(9)
Cu1–O1	2.002(2)	N1′–Cu1–O1	91.47(9)
Cu1–O2	2.492(2)	N1′–Cu1–O1′	165.45(9)
Cu1–O2′	2.492(2)	O1–Cu1–O1′	87.34(1)

The neighboring monomeric units of compound **1** are interconnected via non-covalent C–H···π and π-stacking interactions to form the 1D supramolecular chain along the crystallographic c axis (Figure S1). The –CH moiety (–C4H4) of bz moiety is involved in C–H···π interactions with the π-system of the aromatic ring of Hdmpz having centroid (C9, C10, C11, N1 and N2)···H4 distance of 2.70 Å. The angle between H4, the centroid of the pyrazole ring and the aromatic plane is 159.1° which indicates the strong nature of the interaction [69].

Aromatic π-stacking interactions are observed between the aromatic rings of bz moieties from adjacent monomeric units having centroid(C2-C7)–centroid(C2′-C7′) separation of 3.62 Å. The corresponding slipped angle; the angle between the ring normal and the vector joining the two ring centroids; is found to be 21.5° [70]. Further analysis reveals that neighboring 1D chains shown in Figure S1, interconnect via C–H···π and non-covalent C–H···C interactions to form a layered assembly along the crystallographic ac plane (Figure 2).

Further analysis reveals the formation of another layered architecture of the compound which is stabilized by non-covalent C–H···C; C–H···π; C–H···O, O–H···O and N–H···O hydrogen bonding and aromatic π-stacking interactions along the crystallographic bc plane (Figure 3a). Non-covalent C–H···C interactions are observed between the –CH moieties (–C6H6 and –C7H7) and C5 (from bz) and C8 (from Hdmpz) atoms from two adjacent monomeric units having C6–H6···C8 and C7–H7···C5 distances of 2.94 and 3.11 Å respectively [C6(sp^2)–H6···C8(sp^3); C6···C8 = 3.60Å; C7(sp^2)–H7···C5(sp^2); C7···C5 = 3.79Å]. The –CH moiety (–C12H12A) of Hdmpz is involved in C–H···π interactions with the π-system of the aromatic ring of another Hdmpz moiety from an adjacent monomeric unit having centroid(C9-C11, N1, N2)···H12A distance of 3.04 Å. The angle between H12A, the centroid of the Hdmpz moiety and the aromatic plane is 150.2° which evidences the strong nature of the interaction [71–73]. C–H···O hydrogen bonding interactions are observed between the –C12H12A moiety of Hdmpz and uncoordinated carboxyl atom (O3) of bz from two neighboring units having C12–H12A ···O3 distance of 2.95 Å.

 doi:10.20944/preprints202403.0550.v1

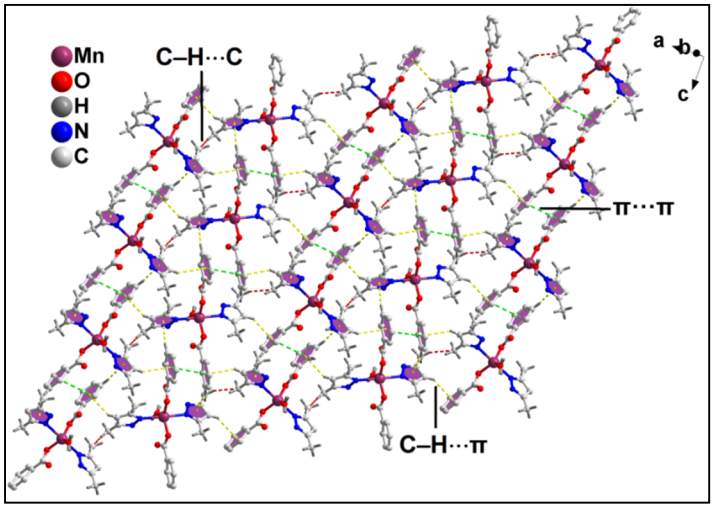

Figure 2. Layered assembly of compound **1** assisted by C–H···π, π-stacking interactions and non-covalent C–H···C interactions along the crystallographic ac plane.

O3 atom of bz moieties are also involved in N–H···O hydrogen bonding interactions with –N2H2 fragments from Hdmpz moieties of adjacent monomeric units having N2–H2···O3 distance of 2.10 Å. Moreover, O3 atom of bz are also involved in O–H···O hydrogen bonding interactions with the coordinated water molecule having O1–H1A···O3 distance of 1.86 Å. A self-assembled dimer [Figure 3(b)] retrieved from the layered architecture along this plane has been theoretically studied (vide infra).

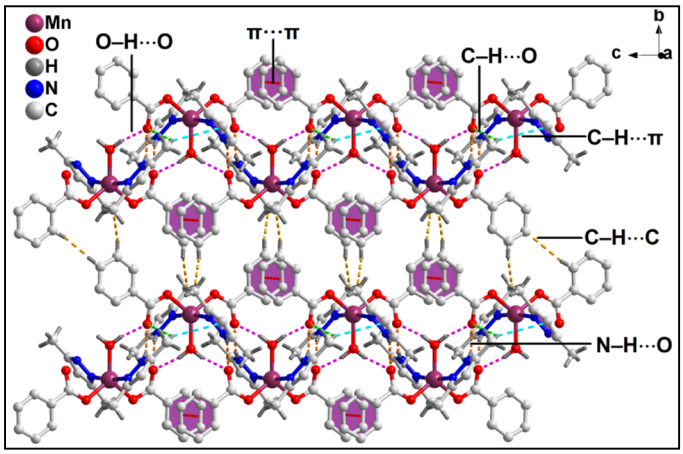

(**a**)

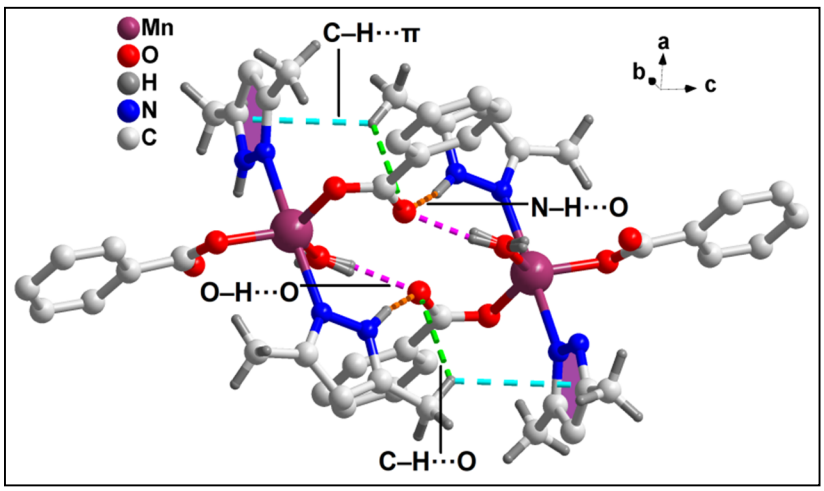

 doi:10.20944/preprints202403.0550.v1

(**b**)

Figure 3. (**a**) Layered architecture of compound **1** involving non-covalent C–H···C; C–H···π; C–H···O, O–H ··· O and N–H ··· O hydrogen bonding and aromatic π-stacking interactions along the crystallographic bc plane; (**b**) a self-assembled dimer retrieved from the layered architecture which is theoretically studied.

Figure 4 depicts the molecular structure of compound **2**. Compound **2** crystallizes in orthorhombic crystal system with Pbcn space group. Selected bond lengths and bond angles have been summarized in Table 2. In compound **2**, the Cu1 metal centre is hexa-coordinated to two bidentate crot moieties and two monodentate Hdmpz moieties. The coordination geometry around the metal centre is slightly distorted octahedron where the axial sites are occupied by O1′ and N1′ atoms from crot and Hdmpz moieties respectively while the equatorial sites are occupied by O1, O2, O2′ from crot and N1 from Hdmpz respectively. The average Cu–O and Cu–N bond distances are almost consistent with the previously reported Cu(II) complexes [74].

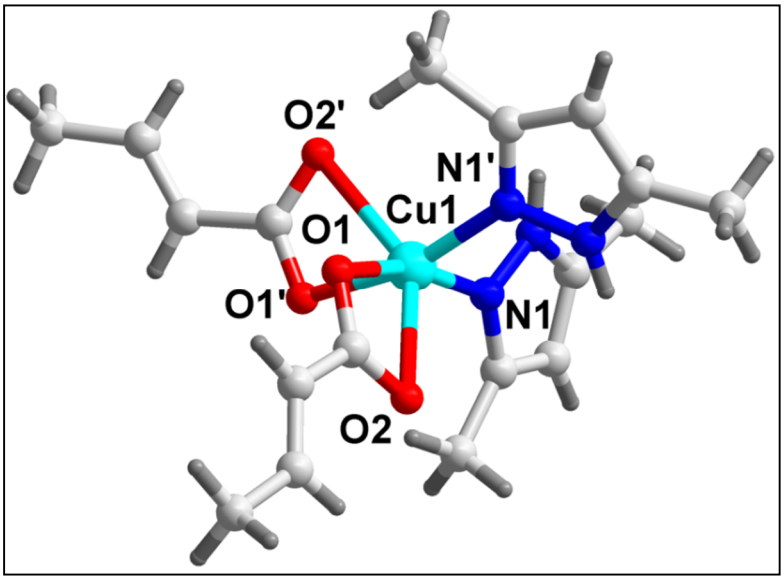

Figure 4. Molecular structure of [Cu(Crot)$_2$(Hdmpz)$_2$] (**2**).

The neighboring monomeric units of compound **2** are interconnected via non-covalent C–H···C interactions to form the 1D supramolecular chain of the compound (Figure S2). C–H···C interactions are observed between the –CH (–C9H9C and –C2H2B) and carbon atoms (C2 and C9) of crot moieties having C9–H9C···C2and C2–H2B···C9 distances of 2.88 and 3.05 Å respectively [C9(sp^3)–H9C···C2(sp^3); C2(sp^3)–H2B···C9(sp^3); C9···C2 = 3.78 Å].

Moreover, two neighboring 1D chains of the compound are interconnected via non-covalent C–H···C interactions to form the 2D layered assembly of the compound (Figure 5). C–H···C interaction is observed between the –CH moiety (–C3H3) of Hdmpz and C7 atom of crot with C3–H3···C7 distance of 3.63 Å [C3(sp^2)–H3···C7(sp^2); C3···C7 = 3.86 Å].

Figure 6(a) depicts another supramolecular 1D chain of compound 2 stabilized by N–H···O hydrogen bonding and aromatic π-stacking interactions. N–H···O hydrogen bonding interaction is observed between the –N2H2 moiety of Hdmpz and O2 atom of crot from two different monomeric units having N2–H2···O2 distance of 1.90 Å. Aromatic π-stacking interactions are observed between the π systems of Hdmpz and crot moieties from adjacent monomeric units of the compound having centroid (C1, C3, C4, N1, N2)–centroid(C7-C8) distance and the corresponding slipped angle of 3.92 Å and 19.1° respectively. A self-assembled dimer [Figure 6(b)] retrieved from the 1D self-assembly along the crystallographic c axis has been theoretically studied (vide infra).

 doi:10.20944/preprints202403.0550.v1

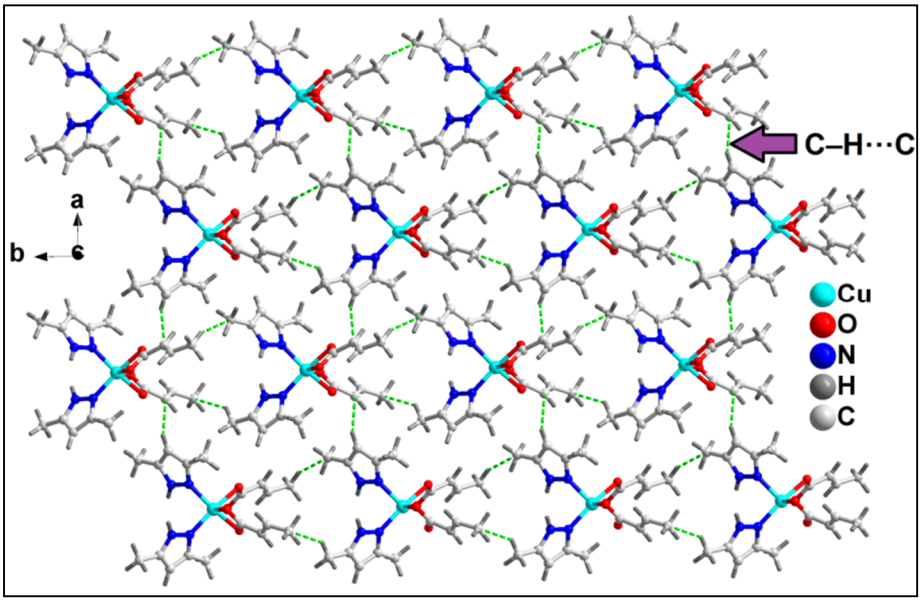

Figure 5. Layered assembly of compound **2** stabilized by non-covalent C–H···C interactions along the crystallographic ab plane.

These 1D supramolecular chains are interconnected via non-covalent C–H···C interactions and C–H···O hydrogen bonding to form a layered assembly along the crystallographic bc plane (Figure 7). Non-covalent C–H···C interactions are observed between the –C9H9C, –C7H7 fragments and C2, C7, C9 atoms of crot moieties from adjacent monomeric units with C9–H9C···C7, C7–H7···C9 and C9–H9C···C2 separations of 3.93, 3.97 and 2.88 Å respectively [C9(sp^3); C7(sp^2); C2(sp^3); C9···C7 = 3.76 Å; C9···C2 = 3.78 Å]. Moreover, C–H···O hydrogen bonding interaction is observed between the –C9H9A fragment and O1 atom of adjacent crot moieties having C9–H9A···O1 distance of 3.07 Å.

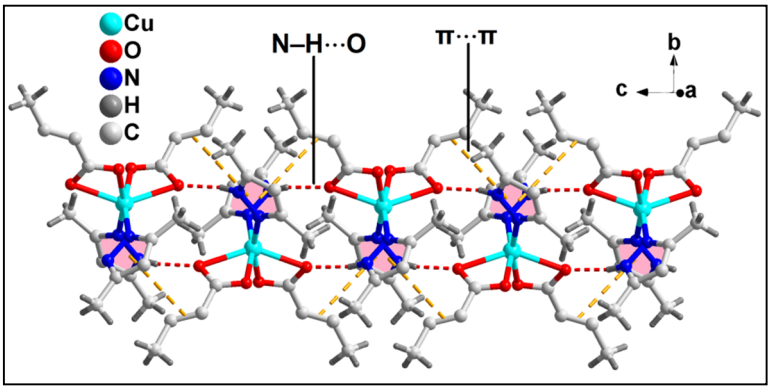

(**a**)

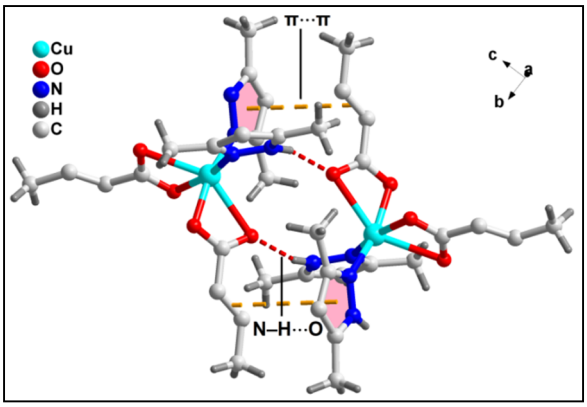

(**b**)

 doi:10.20944/preprints202403.0550.v1

Figure 6. (**a**) 1D supramolecular chain of compound **2** assisted by N–H···O hydrogen bonding and aromatic π-stacking interactions along the crystallographic c axis; (**b**) a self-assembled dimer retrieved from the 1D chain which is theoretically studied.

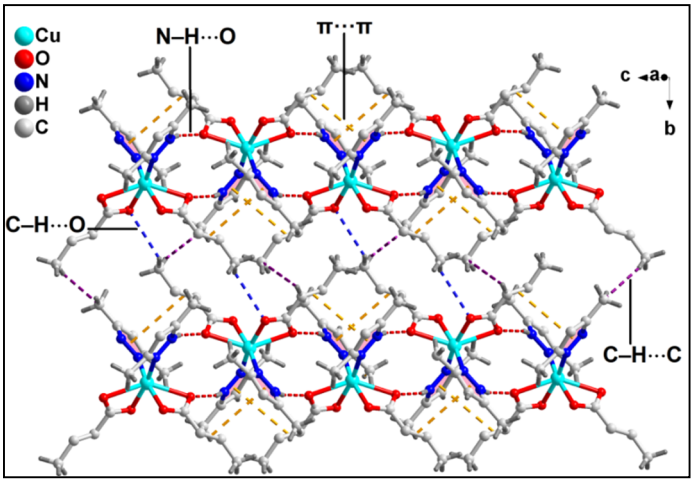

Figure 7. Layered assembly of compound **2** assisted by non-covalent C–H···C; N–H···O and C–H···O hydrogen bonding and aromatic π-stacking interactions along the crystallographic bc plane.

Table 3. Selected hydrogen bond distances (Å) and angles (°) for **1** and **2.**

D–H···A	d(D–H)	d(D···A)	d(H···A)	<(DHA)
1				
C12–H12A···O3	0.98	3.64(3)	2.95(1)	128.6
N2–H2···O3	0.88	2.91(2)	2.10(1)	153.7
O1–H1A···O3	0.87	2.70(2)	1.86(2)	164.1
2				
N2–H2···O2	0.88	2.74(3)	1.90(2)	157.2
C9–H9A···O1	0.98	3.57(4)	3.07(2)	113.2

3.3. Spectral studies

3.3.1. FT-IR spectroscopy

The FT-IR spectra of compounds **1** and **2** (KBr phase) were recorded in the region 4000-500 cm^{-1} (Figure S3). The comparatively broad absorption peak in compound **1** at around 3440 cm^{-1} can be attributed to the O–H stretching vibrations of the coordinated water molecule present in the compound [75,76]. FT-IR spectrum of compound **1** exhibits absorption bands due to $_r$ (H_2O) (715 cm^{-1}) and $_w$ (H_2O) (655 cm^{-1}) which supports the presence of coordinated water molecule in the compound [75,76]. For compound **1**, strong absorption bands appear at 1593 and 1389 cm^{-1} for the asymmetric and symmetric stretching vibrations of the carboxylate groups of bz moiety respectively [77]. The difference between the asymmetric and symmetric stretching vibrations (v = 204 cm^{-1}) of the carboxyl groups of bz moieties of **1** indicates monodentate coordination of the carboxylate moieties to the metal centre [78]. Similarly, for compound **2**, strong absorption bands appear at 1593 and 1414 cm^{-1} for the asymmetric and symmetric stretching vibrations of the carboxylate groups of crot moiety respectively [77]. The difference between the asymmetric and symmetric stretching vibrations (v = 179 cm^{-1}) of the carboxyl groups of crot moieties of **2** indicates bidentate coordination of the carboxylate moieties to the metal centre [78]. The absence of a sharp band at 1710 cm^{-1} for compounds **1** and **2** indicates the deprotonation of the carboxyl groups upon coordination with the

 doi:10.20944/preprints202403.0550.v1

metal centre [80–82]. Moreover, for both the compounds, bands at around 3130 cm^{-1} can be assigned to the ν(N–H) vibrations of coordinated Hdmpz moieties [83,84]. The ν(C–H) vibrations of the coordinated Hdmpz are observed in the region of 2970-2770 cm^{-1} for both the compounds [85]. The peaks at 1429, 1280 and 1145cm^{-1} in **1** can be attributed to the C–N, N–N and C = N stretching vibrations of Hdmpz rings respectively; however, these peaks are obtained at 1430, 1288 and 1150 cm^{-1}in the spectrum of compound **2** [86].

3.3.2. Electronic spectroscopy

The electronic spectra of the compounds have been recorded in both solid and in aqueous phases (Figures S4 and S5). The solid state UV-Vis-NIR spectrum of compound **1** show no absorption bands in the visible region, as the Mn(II) centre (d^5 system) has all the electronic transitions from the $^6A_{1g}$ ground state doubly forbidden [87]. The peaks for π→π* absorption of the benzoate and Hdmpz ligands are obtained at the expected positions [88,89].

The solid state UV-Vis-NIR spectrum of compound **2** (Figure S5) exhibits peaks at 228 and 273 nm assigned to π→π* transitions of the aromatic ligand [90]. The spectrum (Figure S5a) shows broad absorption band at 741 nm resulting from the usual $^2E_g \rightarrow {}^2T_{2g}$ transition for Cu(II) complexes [91]. In the UV-Vis spectra (Figure S5b) of the compound, the absorption peaks for n→π* and $^2E_g \rightarrow {}^2T_{2g}$ transitions are obtained at the expected positions [91].

The similar absorption bands observed in the solid and solution phase electronic spectra of the compounds indicate that the compounds do not undergo any structural deformaion in the aqueous phase [92].

3.4. Thermogravimetric analysis

Thermogravimetric curves of the compounds **1** and **2** were obtained in the temperature range 30-800°C at the heating rate of 10°C/min under N_2 atmosphere (Figure S6). In **1**; the temperature range 120-140°C attributes to the weight loss of coordinated water molecule, (obs. = 5.1%; calcd. = 3.54%) [93,94]. In the temperature range 141-260°C, there is the decomposition of two benzoate moieties and one Hdmpz molecule (obs. = 65.52%; calcd. = 66.61%) [93,94]. For compound **2**; in the temperature range 120-170°C, one coordinated crot undergoes thermal decomposition with the observed weight loss of 18.40% (calcd. = 19.95%) [98]. One coordinated Hdmpz and another coordinated crot are lost in 171-290°C with the observed weight loss of 40.5% (calcd. 42.45%) [97,98]. Finally, loss of the remaining coordinated Hdmpz in the temperature range 291-370°C is observed with the observed weight loss of 24.4% (calcd. = 22.5%) [99].

3.5. Theoretical studies

The aim of this theoretical study is to analyze the non-covalent interactions present in the solid state of the compounds, which remarkably influence their X-ray structure. In addition to weak non-covalent interactions such as π-stacking and C–H···π interactions (see Figures 3 and 7), we have evaluated the H-bonding interactions as they are involved in the formation of interesting 1D assemblies in the solid state of both compounds (see Figure 8) and focused on the comparison of the energetic features of C–H···O, N–H···O, and O–H···O H bonding interactions.

 doi:10.20944/preprints202403.0550.v1

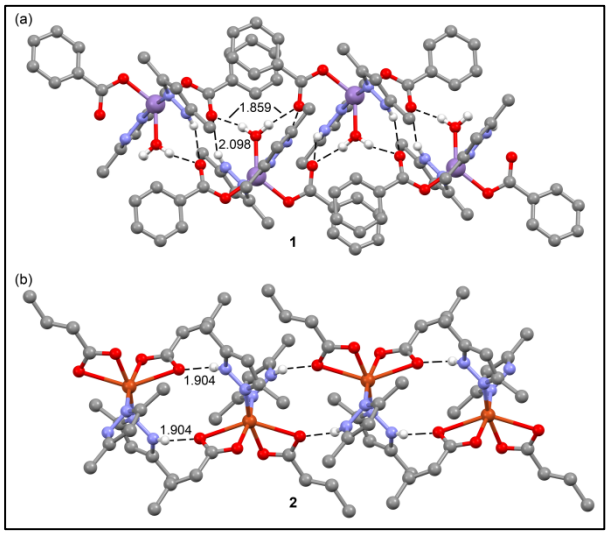

Figure 8. Partial view of the 1D infinite supramolecular chains observed in the solid state of compounds 1 (a) and 2 (b). Distances are in Å. The H-atoms have been omitted, apart from those participating in the O–H···O and N–H···O H-bonds.

We have computed the molecular electrostatic potential (MEP) surfaces of compounds **1** and **2** to investigate the most electrophilic and nucleophilic parts of the compounds. The surfaces, depicted in Figure 9, show that in compound **1**, the MEP maximum is located at the H-atoms of the coordinated water molecule (65.9 kcal/mol), followed by the –NH group (61.5 kcal/mol) of the Hdmpz ligand. Such large MEP values are observed due to the enhanced acidity of the OH_2 and –NH protons upon coordination to the Mn(II) metal center. This result anticipates that the water molecule is a better H-bond donor in comparison to the pyrazole ring. The MEP minimum is located at the non-coordinated O-atom of the benzoate ligand. The MEP is positive at the H-atoms of the methyl groups (~18.8 kcal/mol) and negative at the benzoate and pyrazole π-systems (–23.8 kcal/mol and –8.2 kcal/mol respectively). However, for compound **2**, the MEP maximum is located at the –NH group (51.5 kcal/mol) of the Hdmpz ligand, and the minimum at the O-atom of the crotonate ligand (–53.3 kcal/mol). The MEP is large and negative at the π-system of the double bond. The MEP value at the H-atom of the methyl group is positive (18.9 kcal/mol) and slightly positive at the π-system of the pyrazole ligand (6.3 kcal/mol), showing a differentiating feature with respect to compound **1**.

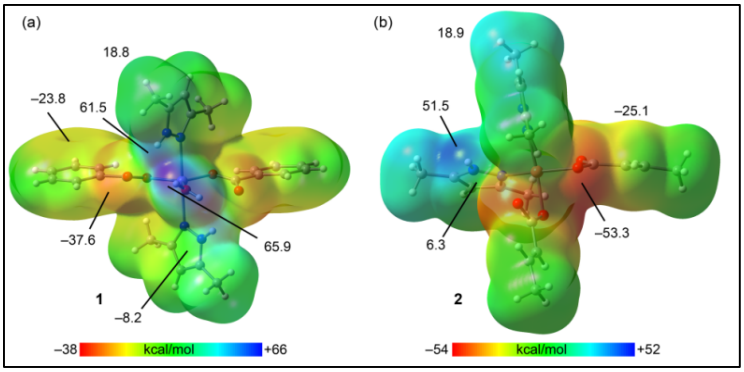

Figure 9. MEP surfaces of compounds **1** (a) and **2** (b). Isovalue: 0.001 a.u. Energies are given in kcal/mol.

We have also analyzed two dimeric assemblies of compound **1** as depicted in Figure 10. These assemblies are intended to analyze both the H-bonds and π-interactions, which are relevant in the solid state (see Figures 3(a) and S1 respectively). To illustrate the interactions in real space, we have combined QTAIM and NCI plot analyses. The NCI plot analysis utilized color-coded reduced density

 doi:10.20944/preprints202403.0550.v1

gradient (RDG) isosurfaces to reveal the relative strength of the interactions in which, green and blue represent weaker and stronger attractive interactions respectively. Figure 10a shows the combined QTAIM/NCI plot analysis of the H-bonded dimer retrieved from assembly shown in Figures S1 and 3(a). It can be observed that the non-coordinated O-atom of the benzoate ring of one monomer establishes three H-bonds with the other monomer. Therefore, a total of six H-bonds stabilize each dimer. Each H-bond is characterized by a bond critical point (BCP, pink sphere), a bond path (dashed bond), and a reduced density gradient (RDG) disk-shape isosurface. It can be observed that the RDG colors characterizing the O–H···O, N–H···O and C–H···O interactions are dark blue (strong), light blue (moderately strong), and green (weak) respectively. This agrees well with the results obtained via MEP surface analysis and confirms that O–H···O H-bonds are stronger than N–H···O H-bonds. The contribution of each type of H-bond has also been estimated using the QTAIM data at the BCPs that characterize the H-bonds (by means of the potential energy density). It can be observed that the major contribution is from O–H···O (–14.2 kcal/mol), followed by N–H···O (–7.5 kcal/mol), and finally C–H···O (–1.3 kcal/mol). The total contribution of the H-bonds is –23.0 kcal/mol, which is similar to the total binding energy (–25.1 kcal/mol). The difference can be mainly attributed to the C–H···π (pyrazole) interactions that are disclosed by the QTAIM/NCI plot analysis. The contribution of both symmetrically equivalent C–H···π interactions is –2.1 kcal/mol, in line with the small MEP value at the pyrazole ring. On the other hand, Figure 10b displays a large and green RDG isosurface situated between the π-clouds of the coordinated benzoate rings, indicating the presence of π-stacking interactions. This is supported by two BCPs and bond paths interconnecting the carbon atoms of both aromatic rings. The binding energy of this assembly is moderately strong (–8.5 kcal/mol). The QTAIM/NCI Plot analysis also confirms the existence of two symmetrically equivalent C–H···π interactions, characterized by the corresponding BCPs, bond paths, and green RDG isosurfaces. The contribution of the C–H···π interactions is –1.8 kcal/mol, thus suggesting that π-stacking interaction is dominant in this dimer.

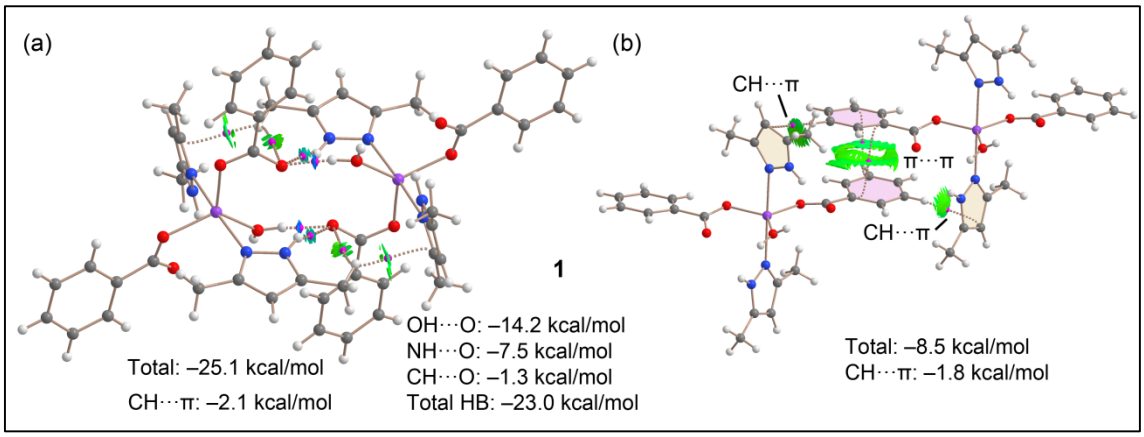

Figure 10. QTAIM (bond CPs in red and bond paths as dashed bonds) and QTAIM (RGD = 0.5, cu-off = 0.035 a.u., color scale: –0.035 a.u. ≤ (signλ_2)*ϱ ≤ 0.035 a.u.) of H-bonded (a) and π···π/CH···π (b) dimers of compound **1**. Only intermolecular interactions are represented.

For compound **2**, the DFT study focuses on the H-bonded dimer retrieved from the 1D infinite chain shown in Figure 6(a) as they play a crucial role in the packing of compound **2**. The N–H···O H-bonds are characterized by BCPs, bond paths, and dark blue RDG isosurfaces, confirming the strong nature of the interactions (see Figure 11)

 doi:10.20944/preprints202403.0550.v1

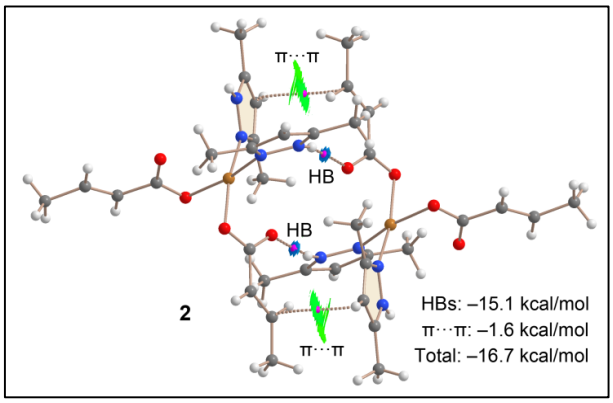

Figure 11. QTAIM (bond CPs in red and bond paths as dashed bonds lines) and QTAIM (RGD = 0.5, cu-off = 0.035 a.u., color scale: –0.035 a.u. ≤ (signλ_2)*ϱ ≤ 0.035 a.u.) of the assembly of compound 2. Only intermolecular interactions are represented.

The strong nature of such interactions is also corroborated by the H-bond energy, which is found to be –15.1 kcal/mol. As shown in Figure 11, a significant RDG isosurface is observed between the π-acidic surface of the coordinated pyrazole ring and the π-basic double bond of the crotonate, in good agreement with the MEP surface analysis. This is further characterized by a BCP and bond path connecting one carbon atom of the double bond to one C-atom of the aromatic ring. The total binding energy of this dimer is moderately strong (–16.7 kcal/mol) and dominated by the H-bonds since the contribution of the π···π interaction is very modest (–1.6 kcal/mol).

4. Conclusions

Two new coordination compounds of Mn(II) and Cu(II) *viz*. [Mn(bz)$_2$(Hdmpz)$_2$(H$_2$O)] (**1**) and [Cu(crot)$_2$(Hdmpz)$_2$] (**2**) have been synthesized and characterized using single crystal X-ray diffraction technique, FT-IR, electronic spectroscopy, TGA and elemental analyses. Compound **1** is a penta-coordinated Mn(II) mononuclear compound; whereas, compound **2** crystallizes as hexa-coordinated Cu(II) compound of *Hdmpz*. Crystal structure analysis of compound **1** reveals the existence of C–H···π and π-stacking interactions which stabilizes the layered architecture of the compound along with the dominant O–H···O, N–H···O and C–H···O H-bonding interactions. The presence of aromatic π-stacking (between π ring of pyrazole and π double bond of crotonate), along with non-covalent C–H···O and N–H···O hydrogen bonding interactions stabilizes the crystal structure of compound **2**. Theoretical study has delved into the non-covalent interactions in compounds **1** and **2**, focusing on hydrogen bonds in solid-state structures and π-interactions (π···π and C–H···π). Molecular electrostatic potential (MEP) surfaces show that the coordinated water molecule and –NH group of *Hdmpz* are the primary H-bond donors. QTAIM and NCI plot analyses highlighted the nature and strength of these interactions. Results confirmed strong O–H···O and N–H···O hydrogen bonds and much weaker C–H···O, π···π and C–H···π interactions.

Supplementary Materials: The following supporting information can be downloaded at the website of this paper posted on Preprints.org, Figures S1–S6, Figure S1: 1D chain of compound **1** involving intermolecular C–H···π and π-stacking interactions along the crystallographic c axis; Figure S2: 1D supramolecular chain of compound **2** assisted by non-covalent C–H···C interactions along the crystallographic b axis; Figure S3: FT-IR spectra of compounds **1** and **2**; Figure S4: (a) UV-Vis-NIR spectrum of **1**, (b) UV-Vis spectrum of **1**; Figure S5: (a) UV-Vis-NIR spectrum of **2**, (b) UV-Vis spectrum of **2**; Figure S6: Thermogravimetric curves of the compounds **1** and **2**.

Author Contributions: Conceptualization, A.F. and M.K.B.; methodology, A.F. and M.K.B.; software, A.F. formal analysis, A.F.; investigation, M.B. and T.B.; data curation, M.B.-O.; writing—original draft preparation, M.B.; T.B.; and M.K.B.; writing—review and editing, M.K.B.; visualization, A.F.; supervision, M.K.B.; project administration, A.F. and M.K.B.; funding acquisition, A.F. and M.K.B. All authors have read and agreed to the published version of the manuscript.

Funding: Financial support was provided by SERB-SURE (Grant number: SUR/2022/001262), ASTEC, DST, Govt. of Assam (grant number ASTEC/S&T/192(177)/2020-2021/43) and the Gobierno de Espana, MICIU/AEI (project number PID2020-115637GB-I00), all of whom are gratefully acknowledged. The authors thank IIT-Guwahati for the TG data.

Data Availability Statement: Not applicable

Conflicts of Interest: The authors declare no conflict of interest. The funders had no role in the design of the study; in the collection, analyses, or interpretation of data; in the writing of the manuscript; or in the decision to publish the results.

References

1. Li, H.-Y.; Zhao, S.-N.; Zang, S.-Q.; Li, J. Functional Metal–Organic Frameworks as Effective Sensors of Gases and Volatile Compounds. *Chem. Soc. Rev.* **2020**, *49*, 6364–6401.
2. Lin, J.; Ho, W.; Qin, X.; Leung, C.-F.; Au, V.K.-M.; Lee, S. Metal–Organic Frameworks for NOx Adsorption and Their Applications in Separation, Sensing, Catalysis, and Biology. *Small* **2022**, *18*, 2105484-2105498.
3. Xie, L.S.; Skorupskii, G.; Dincă, M. Electrically Conductive Metal–Organic Frameworks. *Chem. Rev.* **2020**, *120*, 8536–8580.
4. Hambley, T.W. Developing new metal-based therapeutics: challenges and opportunities. *Dalton Trans*. **2007**, 4929–4937.
5. Thompson, K.H.; Orvig, C. Metal complexes in medicinal chemistry: new vistas and challenges in drug design. *Dalton Trans*. **2006**, 761–764.
6. Wang, H.; Hamanaka, S.; Nishimoto, Y.; Irle, S.; Yokoyama, T.; Yoshikawa, H.; Awaga, K. In Operando X-ray Absorption Fine Structure Studies of Polyoxometalate Molecular Cluster Batteries: Polyoxometalates as Electron Sponges. *J. Am. Chem. Soc*. **2012**, *134*, 4918-4928.
7. Swieger, G. F.; Malefetse, T. J. New Self-Assembled Structural Motifs in Coordination Chemistry. *Chem. Rev*. **2000**, *100*, 3483-3495.
8. Koohpayeh, S.M. Single Crystal Growth by the Traveling Solvent Technique: A Review. *Progress in Crystal Growth and Characterization of Materials* **2016**, *62*, 22–34.
9. Aakeroy, C.B.; Champness, N.R.; Janiak, C. Recent advances in crystal engineering. *CrystEngComm*. **2012**, *12*, 22-40.
10. Calvin, J.J.; Brewer, A.S.; Alivisatos, A.P. The Role of Organic Ligand Shell Structures in Colloidal Nanocrystal Synthesis. *Nat Synth* **2022**, *1*, 127–137.
11. Schiebi, J.; Schulmeister, J.; Doppiu, A.; Worner, E.; Rudolph, M.; Karch, R.; Hashmi, A. S.K. An Industrial Perspective on Counter Anions in Gold Catalysis: On Alternative Counter Anions. *Adv. Synth. Catal*. **2018**, *360*, 3949-3965.
12. Khavasi, H.R.; Sadegh, B.M.M. Temperature-Dependent Supramolecular Motif in Coordination Compounds. *Inorg. Chem*. **2010**, 49, 5356-5370.
13. He, L.; Li, W.; Jiang, Z.W.; Zhao, T.T.; Li, Y.; Li, C.M.; Huang, C.Z.; Li, Y.F. Novel solvent-triggered transformation of Cu-based metal-organic gels to highly monodisperse metal-organic frameworks with controllable shapes. *Chem. Eng. J*. **2019**, *374*, 1231.
14. Chen, H.; Fraser Stoddart, J. From Molecular to Supramolecular Electronics. *Nat Rev Mater* **2021**, *6*, 804–828.
15. Hobza, P.; Zahradník, R.; Müller-Dethlefs, K. The World of Non-Covalent Interactions: 2006. *Collect. Czech. Chem. Commun*. **2006**, *71*, 443–531.
16. Lackinger, M.; Heckl, W. M. Langmuir. Carboxylic Acids: Versatile Building Blocks and Mediators for Two-Dimensional Supramolecular Self-Assembly.*Langmuir*. **2009,** *25*, 11307–11321.
17. Batten, S.R.; Neville, S.M.; Turner, D.R. *Coordination Polymers: Design, Analysis and Application*. Royal Society of Chemistry: Cambridge, **2009**.
18. Hong, M.C.; Chen, L. *Design and Construction of Coordination Polymers*. John Wiley: Hoboken, NJ, **2009**.
19. Politzer, P.; Murray, J.S.; Clark, T. Halogen bonding and other σ-hole interactions: a perspective. *Phys. Chem. Chem. Phys*. **2013**, *15*, 11178-11190.
20. Bauza, A.; Mooibroek, T. J.; Frontera, A. Tetrel-Bonding Interaction: Rediscovered Supramolecular Force?. *Angew. Chem. Int. Ed*. **2013**, *52*, 12317-12329.
21. Egli, M.; Sarkhel, S. Lone Pair−Aromatic Interactions: To Stabilize or Not to Stabilize. *Acc. Chem. Res*. **2007**, *40*, 197.
22. Mooibroek, T.J.; Gamez, P.; Reedijk, J. Lone pair–π interactions: a new supramolecular bond?. *CrystEngComm*. **2008**, *10*, 1501-1520.
23. Kumar, P.; Banerjee, S.; Radha, A.; Firdoos, T.; Sahoo, S.C.; Pandey, S.K. Role of Non-Covalent Interactions in the Supramolecular Architectures of Mercury(II) Diphenyldithiophosphates: An Experimental and Theoretical Investigation. *New J. Chem.* **2021**, *45*, 2249–2263.

24. Reeda, V.J.; Sakthivel, S.; Divya, P.; Javed, S.; Jothy, V.B. Conformational Stability, Quantum Computational (DFT), Vibrational, Electronic and Non-Covalent Interactions (QTAIM, RDG and IGM) of Antibacterial Compound N-(1-Naphthyl)Ethylenediamine Dihydrochloride. *J. Mol. Struct.* **2024**, *1298*, 137043-137060.
25. Wheeler, S.E.; McNeil, A.J.; Muller, P.; Swager, T.M.; Houk, K.N. Probing Substituent Effects in Aryl-Aryl Interactions Using Stereoselective Diels-Alder Cycloadditions *J. Am. Chem. Soc.* **2010**, *132*, 3304–3311.
26. Verevkin, S.P.; Kondratev, S.O.; Zaitsau, D.H.; Zherikova, K.V.; Ludwig, R. Quantification and Understanding of Non-Covalent Interactions in Molecular and Ionic Systems: Dispersion Interactions and Hydrogen Bonding Analysed by Thermodynamic Methods. *J. Mol. Liq.* **2021**, *343*, 117547-117560.
27. Park, T.; Zimmerman, S.C.; Nakashima, S. A Highly Stable Quadruply Hydrogen-Bonded Heterocomplex Useful for Supramolecular Polymer Blends. *J. Am. Chem. Soc.* **2005**, *127*, 6520-6536.
28. Pu, L.-M.; An, X.-X.; Liu, C.; Long, H.-T.; Zhao, L. Insights into Crystal Structures, Supramolecular Architectures and Antioxidant Activities of Self-Assembled Fluorescent Hetero-Multinuclear [Cu (II)-Ln (III)] (Ln = La, Ce, Pr and Nd) Salamo-like Complexes. *Appl. Organomet. Chem.* **2020**, *34*, 5980-5995.
29. Banerjee, A.; Mukherjee, P.S. Chapter Nine - Self-Assembled Discrete Coordination Architectures toward Biological Applications. In *Adv. Inorg. Chem.*; Academic Press, **2023**, *81*, 345–387.
30. Cai, H.-Q.; Liu, C.-H.; Xin, Y.; Wang, C.; Bai, F.-Y.; Sun, L.-X.; Xing, Y.-H. Construction of Poly-Iodine Aromatic Carboxylate Mn/Co Frameworks and Iodine Adsorption Behavior. *Transit Met Chem* **2021**, *46*, 633–644.
31. Nath, H.; Dutta, D.; Sharma, P.; Frontera, A.; Verma, A. K.; Barcelo´-Oliver, M.; Devi, M.; Bhattacharyya, M. K. Adipato bridged novel hexanuclear Cu(ii) and polymeric Co(ii) coordination compounds involving cooperative supramolecular assemblies and encapsulated guest water clusters in a square grid host: antiproliferative evaluation and theoretical studies. *Dalton Trans.* **2020**, *49*, 9863–9881.
32. Xu, Z.-H.; Huang, Z.-Q.; Liu, X.-H.; Zhao, Y.; Lu, Y.; Sun, W.-Y. Luminescent Silver(I) Complexes with Pyrazole-Tetraphenylethene Ligands: Turn-on Fluorescence Due to the Coordination-Driven Rigidification and Solvent-Oriented Structural Transformation. *Dalton Trans.* **2021**, *50*, 2183–2191.
33. Lunagariya, M.V.; Thakor, K.P.; Varma, R.R.; Waghela, B.N.; Pathak, C.; Patel, M. N. Synthesis, characterization and biological application of 5-quinoline 1,3,5-trisubstituted pyrazole based platinum(ii) complexes. *MedChemComm* **2018**, *9*, 282.
34. Dias, I.M.; Junior, H.C.S.; Costa, S.C.; Cardoso, C.M.; Cruz, A.G.B.; Santos, C.E.R.; Candela, D.R.S.; Soriano, S.; Marques, M.M.; Ferreira, G.B.; et al. Mononuclear Coordination Compounds Containing a Pyrazole-Based Ligand: Syntheses, Magnetism and Acetylcholinesterase Inhibition Assays. *J. Mol. Struct.* **2020**, *1205*, 127564-127579.
35. Bouroumane, N.; El Kodadi, M.; Touzani, R.; El Boutaybi, M.; Oussaid, A.; Hammouti, B.; Nandiyanto, A.B.D. New Pyrazole-Based Ligands: Synthesis, Characterization, and Catalytic Activity of Their Copper Complexes. *Arab J Sci Eng* **2022**, *47*, 269–279.
36. Draoui, Y.; Radi, S.; Tanan, A.; Oulmidi, A.; N. Miras, H.; Benabbes, R.; Ouahhoudo, S.; Mamri, S.; Rotaru, A.; Garcia, Y. Novel Family of Bis-Pyrazole Coordination Complexes as Potent Antibacterial and Antifungal Agents. *RSC Advances* **2022**, *12*, 17755–17764.
37. Abdolmaleki, S.; Ghadermazi, M.; Fattahi, A.; Shokraii, S.; Alimoradi, M.; Shahbazi, B.; Azar, A.R.J. Synthesis, crystallographic and spectroscopic studies, evaluation as antimicrobial and cytotoxic agents of a novel mixed-ligand nickel(II) complex. *J. Coord. Chem.* **2017**, *70*, 1406-1422.
38. Draoui, Y.; Radi, S.; Tanan, A.; Oulmidi, A.; N. Miras, H.; Benabbes, R.; Ouahhoudo, S.; Mamri, S.; Rotaru, A.; Garcia, Y. Novel Family of Bis-Pyrazole Coordination Complexes as Potent Antibacterial and Antifungal Agents. *RSC Advances* **2022**, *12*, 17755–17764.
39. Alam, M.J.; Alam, O.; Naim, M.J.; Nawaz, F.; Manaithiya, A.; Imran, M.; Thabet, H.K.; Alshehri, S.; Ghoneim, M.M.; Alam, P.; et al. Recent Advancement in Drug Design and Discovery of Pyrazole Biomolecules as Cancer and Inflammation Therapeutics. *Molecules* **2022**, *27*, 8708-8719.
40. Harit, T.; Malek, F.; El Bali, B.; Khan, A.; Dalvandi, K.; Marasini, B.P.; Noreen, S.; Malik, R.; Khan, S.; Choudhary, M.I. Synthesis and enzyme inhibitory activities of some new pyrazole-based heterocyclic compounds. *Med. Chem. Res.* **2012**, *21*, 2772-2778.
41. Li, G.; Cheng, Y.; Han, C.; Song, C.; Huang, N.; Du, Y. Pyrazole-Containing Pharmaceuticals: Target, Pharmacological Activity, and Their SAR Studies. *RSC Med. Chem.* **2022**, *13*, 1300–1321.
42. Chauhan, A.; Sharma, P.K.; Kaushik, N. Pyrazole: A Versatile Moiety. *Int. J. Chem. Technol. Res.* **2011**, *3*, 11-32.
43. Shagufta; Ahmad, I. Transition Metal Complexes as Proteasome Inhibitors for Cancer Treatment. *Inorganica Chim. Acta* **2020**, *506*, 119521-119535.
44. Li, J.; Chen, T. Transition Metal Complexes as Photosensitizers for Integrated Cancer Theranostic Applications. Coordination *Chem. Rev.* **2020**, *418*, 213355-213370.
45. Imberti, C.; Zhang, P.; Huang, H.; Sadler, P.J. New Designs for Phototherapeutic Transition Metal Complexes. *Angew. Chem. Int. Ed.* **2020**, *59*, 61–73.

46. Permyakov, E.A. Metal Binding Proteins. *Encyclopedia* **2021**, *1*, 261–292.
47. Salih, B.D.; Dalaf, A.H.; Alheety, M.A.; Rashed, W.M.; Abdullah, I.Q. Biological Activity and Laser Efficacy of New Co (II), Ni (II), Cu (II), Mn (II) and Zn (II) Complexes with Phthalic Anhydride. *Materials Today: Proceedings* **2021**, *43*, 869–874.
48. Bouzerafa, B.; Ourari, A.; Aggoun, D.; Ruiz-Rosas, R.; Ouennoughi, Y.; Morallon, E. Novel nickel(II) and manganese(III) complexes with bidentate Schiff-base ligand: synthesis, spectral, thermogravimetry, electrochemical and electrocatalytical properties. *Res. Chem. Intermed*. **2016**, *42*, 4839–4858.
49. Osypiuk, D.; Cristóvão, B.; Bartyzel, A. New Coordination Compounds of CuII with Schiff Base Ligands—Crystal Structure, Thermal, and Spectral Investigations. *Crystals* **2020**, *10*, 1004-1120.
50. Barma, A.; Bhattacharjee, A.; Roy, P. Dinuclear Copper(II) Complexes with N,O Donor Ligands: Partial Ligand Hydrolysis and Alcohol Oxidation Catalysis. *Eur. J. of Inorg. Chem.* **2021**, *2021*, 2284–2292.
51. Czylkowska, A.; Rogalewicz, B.; Raducka, A.; Błaszczyk, N.; Maniecki, T.; Wieczorek, K.; Mierczyński, P. Synthesis, Spectroscopic, Thermal and Catalytic Properties of Four New Metal (II) Complexes with Selected N- and O-Donor Ligands. *Materials* **2020**, *13*, 3217-3230.
52. Singh, M.P.; Baruah, J.B. Stable Host–Guest Complexes of Bis-2,6-Pyridinedicarboxylate Iron(III) with Dihydroxybenzenes. *Polyhedron* **2017**, *138*, 103–108.
53. Moriyasu, R.; John, S.G.; Bian, X.; Yang, S.-C.; Moffett, J.W. Cu Exists Predominantly as Kinetically Inert Complexes Throughout the Interior of the Equatorial and North Pacific Ocean. *Global Biogeochemical Cycles* **2023**, *37*, e2022GB007521.
54. SADABS, V2.05; Bruker AXS: Madison, USA, **1999**.
55. Sheldrick, G.M. A Short History of SHELX. *Acta Cryst A* **2008**, *64*, 112–122.
56. Farrugia, L.J. WinGX Suite for Small-Molecule Single-Crystal Crystallography. *J Appl Cryst* **1999**, *32*, 837–838.
57. Brandenburg, K. Diamond 3.1f 2008; Crystal Impact GbR: Bonn, Germany.
58. Gaussian 16, Revision C.01; Frisch, M.J.; Trucks, G.W.; Schlegel, H.B.; Scuseria, G.E.; Robb, M.A.; Cheeseman, J.R.; Scalmani, G.;Barone, V.; Petersson, G.A.; Nakatsuji, H.; Li, X.; Caricato, M.; Marenich, A.V.; Bloino, J.; Janesko, B.G.; Gomperts, R.; Mennucci, B.; Hratchian, H.P.; Ortiz, J.V.; Izmaylov, A.F.; Sonnenberg, J.L.; Williams-Young, D.; Ding, F.; Lipparini, F.; Egidi, F.; Goings, J.; Peng, B.; Petrone, A.; Henderson, T.; Ranasinghe, D.; Zakrzewski, V.G.; Gao, J.; Rega, N.; Zheng, G.; Liang, W.; Hada, M.; Ehara, M.; Toyota, K.; Fukuda, R.; Hasegawa, J.; Ishida, M.; Nakajima, T.; Honda, Y.; Kitao, O.; Nakai, H.; Vreven, T.; Throssell, K.; Montgomery, J. A., Jr.; Peralta, J.E.; Ogliaro, F.; Bearpark, M.J.; Heyd, J.J.; Brothers, E.N.; Kudin, K.N.; Staroverov, V.N.; Keith, T.A.; Kobayashi, R.; Normand, J.; Raghavachari, K.; Rendell, A.P.; Burant, J.C.; Iyengar, S.S.; Tomasi, J.; Cossi, M.; Millam, J.M.; Klene, M.; Adamo, C.; Cammi, R.; Ochterski, J.W.; Martin, R.L.; Morokuma, K.; Farkas, O.; Foresman, J. B.; Fox, D.J. Gaussian, Inc.: Wallingford CT, **2016**.
59. Adamo, C.; Barone, V. Toward reliable density functional methods without adjustable parameters: The PBE0 model. *J. Chem. Phys*. **1999**, *110*, 6158–6170.
60. Grimme, S.; Antony, J.; Ehrlich, S.; Krieg, H. A consistent and accurate ab initio parametrization of density functional dispersion correction (DFT-D) for the 94 elements H-Pu. *J. Chem. Phys.* **2010**, *132*, 154104.
61. Weigend, F. Accurate Coulomb-fitting basis sets for H to Rn. *Phys. Chem. Chem. Phys*. **2006**, *8*, 1057–1065.
62. Bader, R.F.W. A quantum theory of molecular structure and its applications. *Chem. Rev.* **1991**, *91*, 893–928.
63. Johnson, E.R.; Keinan, S.; Mori-Sánchez, P.; Contreras-García, J.; Cohen, A.J.; Yang, W. Revealing Noncovalent Interactions. *J. Am. Chem. Soc*. **2010**, *132*, 6498–6506.
64. AIMAll (Version 19.10.12); Keith, Todd A.; TK Gristmill Software: Overland Park KS, USA, **2019**.
65. Espinosa, E.; Molins, E.; Lecomte, C. Hydrogen bond strengths revealed by topological analyses of experimentally observed electron densities. *Chem. Phys. Lett*. **1998**, *285*, 170-173.
66. Orojloo, M.; Zolgharnein, P.; Solimannejad, M.; Amani, S. Synthesis and characterization of cobalt (II), nickel (II), copper (II) and zinc (II) complexes derived from two Schiff base ligands: Spectroscopic, thermal, magnetic moment, electrochemical and antimicrobial studies. *Inorganica Chim. Acta.* **2017**, *467*, 227-237.
67. Ammar, R.A.; Alaghaz, A.M.A.; Zayed, M.E.; Bedair, L.A.A. Synthesis, spectroscopic, molecular structure, antioxidant, antimicrobial and antitumor behavior of Mn(II), Co(II), Ni(II), Cu(II) and Zn(II) complexes of O_2N type tridentate chromone-2-carboxaldehyde Schiff's base ligand. *J. Mol. Struct*. **2017,** *1141*, 368-381.
68. Psomas, G. Copper(II) and zinc(II) coordination compounds of non-steroidal anti-inflammatory drugs: Structural features and antioxidant activity. *Coord. Chem. Rev*. **2020**, *412*, 213259–213271.
69. Gogoi, A.; Das, A.; Frontera, A.; Verma, A.K.; Bhattacharyya, M.K. Energetically significant unconventional π-π contacts involving fumarate in a novel coordination polymer of Zn(II): In-vitro anticancer evaluation and theoretical studies. *Inorganica Chim. Acta.* **2019**, *493*, 1–13.
70. Janiak, C. A critical account on π–π stacking in metal complexes with aromatic nitrogen-containing ligands. *J. Chem. Soc., Dalton Trans*. **2000**, *21*, 3885–3896.
71. Kokina, T. E.; Glinskaya, L.A.; Tkachev, A.V.; Plyusnin, V.F.; Tsoy, Y.V.; Bagryanskaya, I.Y.; Vasilyev, E. S.; Piryazev, D. A.; Sheludyakova, L. A.; Larionov, S. V. Chiral zinc(II) and cadmium(II) complexes with a

dihydrophenanthroline ligand bearing (–)-α-pinene fragments: Synthesis, crystal structures and photophysical properties. *Polyhedron*. **2016,** 117, 437-444.
72. Das, S.; Bharadwaj, P.K. Self-Assembly of a Luminescent Zinc(II) Complex: a Supramolecular Host–Guest Fluorescence Signaling System for Selective Nitrobenzene Inclusion. *Inorg. Chem.* **2006,** *45*, 5257-5259.
73. Chakravorty, S.; Platts, J.A.; Das, B.K. Novel C–H···C contacts involving 3,5-dimethylpyrazoleligands in a tetracoordinate Co(ii) complex. *Dalton Trans*. **2011**, *40*, 11605-11612.
74. Saha, U.; Dutta, D.; Nath, H.; Franconetti, A.; Frontera, A.; Bhattacharyya, M.K. Supramolecular Association in Cu(II) Coordination Complexes Involving Energetically Significant NO···NO π–Hole Interaction and Cooperative π-Stacked Ternary Assembly: Experimental and Theoretical Studies. *Inorganica Chim. Acta* **2019**, *488*, 159–169
75. Manna, S.C.; Mistri, S.; Jana, A.D. A rare supramolecular assembly involving ion pairs of coordination complexes with a host-guest relationship: synthesis, crystal structure, photoluminescence and thermal study. *CrystEngComm*. **2012**, *14*, 7415-7422.
76. Islam, S.M.N.; Dutta, D.; Guha, A.K.; Bhattacharyya, M.K. An unusual werner type clathrate of Mn(II) benzoate involving energetically significant weak C-H···C contacts: A combined experimental and theoretical study. *J. Mol. Struct*. **2019**, *1175*, 130–138.
77. Nath, H.; Dutta, D.; Sharma, P.; Frontera, A.; Verma, A.K.; Barceló-Oliver, M.; Devi, M.; Bhattacharyya, M.K. Adipato bridged novel hexanuclear Cu(ii) and polymeric Co(ii) coordination compounds involving cooperative supramolecular assemblies and encapsulated guest water clusters in a square grid host: antiproliferative evaluation and theoretical studies. *Dalton Trans*. **2020**, *49*, 9863-9881.
78. Yang, R.; Li, H. H.; Hecke, K. V.; Cui, G. H. Cobalt(II) and Copper(II) Complexes Constructed from Bis(benzimidazole) and 2,6-Pyridinedicarboxylate Co-ligands: Synthesis, Crystal Structures, and Catalytic Properties. *Z. Anorg. Allg. Chem*. **2015**, *641*, 642-649.
79. Goswami, N.; Gogoi, P.K.; Saha, U.; Bhattacharyya, M.K.; Chetia, T.R. Synthesis, Crystal Structure and Application of New Cobalt(II) Complex $[Co(bpy)_2NO_3]\cdot NO_3\cdot 5H_2O$ as Sensitizer in Dye-Sensitized Solar Cells. *Asian J. Chem*. **2018,** *3*, 679–683.
80. Ay, B.; Yildiz, E.; Kani, I. Novel heteroleptic lanthanide organic frameworks containing pyridine-2,5-dicarboxylic acid and in situ generated piperazine-2,5-dicarboxylic acid from piperazine: Hydrothermal synthesis and luminescent properties. *J. Solid State Chem*. **2016**, *233*, 44-51.
81. Yang, L.; Liu, L.; Wu, L.; Zhang, H.; Song, S. A series of 3D isomorphous lanthanide coordination polymers based on flexible dicarboxylate ligand: Synthesis, structure, characterization, and properties. *Dyes Pigm*. **2014**, *105*, 180-191.
82. Łyszczek, R.; Mazur, L. Polynuclear complexes constructed by lanthanides and pyridine-3,5-dicarboxylate ligand: Structures, thermal and luminescent properties. *Polyhedron*. **2012**, *41*, 7-19.
83. Li, J.; Xing, Y.H.; Zhao, H.Y.; Li, Z.P.; Wang, C.G.; Zeng, X.Q.; Ge, M.F.; Niu, S.Y. Constructions of a set of hydrogen-bonded supramolecules from reactions of transition metals with 3,5-dimethylpyrazole and different dicarboxylate ligands. *Inorganica Chim. Acta*. **2009,** *362*, 2788-2795.
84. Lu, Y.; Xu, W.; Hu, K.; Jin, S.; Sun, L.; Liu, B.; Wang, D. Synthesis and structural characterizations of nine non-covalent-bonded Zn^{2+}, and Cd^{2+} supramolecules based on 3,5-dimethylpyrazole and carboxylates. *Polyhedron.* **2019**, *159*, 408-425.
85. Titi, A.; Shiga, T.; Oshio, H.; Touzani, R.; Hammouti, B.; Mouslim, M.; Warad, I. Synthesis of novel Cl2Co4L6 clusterusing 1-hydroxymethyl-3,5-dimethylpyrazole (LH) ligand: Crystal structure, spectral, thermal, Hirschfeld surface analysis and catalytic oxidation evaluation. *J. Mol. Struct.* **2020**, *1199*, 126995-127009.
86. Direm, A.; Tursun, M.; Parlak, C.; Cherif, N.B. Trans-dichlorotetrakis(1H-pyrazole-κN2)copper(II): Synthesis, crystal structure, hydrogen bonding graph-sets, vibrational and DFT studies. *J. Mol. Struct*. **2015**, *1093*, 208-218.
87. Baishya, T.; Sharma, P.; Gomila, R.M.; Frontera, A.; Barcelo-Oliver, M.; Verma, A.K.; Bhattacharyya, M.K. Fumarato and Phthalato Bridged Dinuclear Metal–Organic Cu(II) and Mn(II) Compounds Involving Infinite Fumarate–Water Assemblies and Unusual Structure-Guiding H-Bonded Synthons: Antiproliferative Evaluation and Theoretical Studies. *New J. Chem*. **2022**, *46*, 17817–17833.
88. LEVER, A.B.P. Inorganic Electronic Spectroscopy. *Stud. phys. theor. chem* **1984**, *33*, XVI-863 p.
89. Paul, P.; Roy, S.; Sarkar, S.; Chowdhury, S.; Purkayastha, R.N.D.; Raghavaiah, P.; McArdle, P.; Deb, L.; Devi, S.I. Synthesis, Structure and Some Properties of a Manganese(II) Benzoate Containing Diimine. *J. Mol. Struct.* **2015**, *1102*, 153–160.
90. Silva, P.B. da; Terra, P.H.; Frem, R.C.G.; Netto, A.V.G.; Mauro, A.E. Synthesis, Characterization, and Investigation of the Thermal Behavior of Cu(II) Pyrazolyl Complexes. *J. Therm. Anal. Calorim.*. **2011**, *106*, 495–499.
91. Giles, I.D.; DePriest, J.C.; Deschamps, J.R. Effect of Substitution and the Counterion on the Structural and Spectroscopic Properties of CuII Complexes of Methylated Pyrazoles. *J. Coord. Chem.* **2015**, *68*, 3611–3635.

92. Nath, H.; Dutta, D.; Sharma, P.; Frontera, A.; Verma, A.K.; Barceló-Oliver, M.; Devi, M.; Bhattacharyya, M.K. Adipato Bridged Novel Hexanuclear Cu(II) and Polymeric Co(II) Coordination Compounds Involving Cooperative Supramolecular Assemblies and Encapsulated Guest Water Clusters in a Square Grid Host: Antiproliferative Evaluation and Theoretical Studies. *Dalton Trans.* **2020**, *49*, 9863–9881.
93. Kavitha, N.; Anantha Lakshmi, P.V. Synthesis, Characterization and Thermogravimetric Analysis of Co(II), Ni(II), Cu(II) and Zn(II) Complexes Supported by ONNO Tetradentate Schiff Base Ligand Derived from Hydrazino Benzoxazine. *J. Saudi Chem. Soc.* **2017**, *21*, 457–466.
94. Masoud, M.S.; Ali, A.E.; Elfatah, A.S.A.; Amer, G.E. Synthesis, Molecular Spectroscopy, Computational, Thermal Analysis and Biological Activity of Some Orotic Acid Complexes. *Open J. Inorg.Chem.* **2021**, *11*, 1–22.
95. Sharma, P.; Dutta, D.; Gomila, R.M.; Frontera, A.; Barcelo-Oliver, M.; Verma, A.K.; Bhattacharyya, M.K. Benzoato Bridged Dinuclear Mn(II) and Cu(II) Compounds Involving Guest Chlorobenzoates and Dimeric Paddle Wheel Supramolecular Assemblies: Antiproliferative Evaluation and Theoretical Studies. *Polyhedron* **2021**, *208*, 115409-115422.
96. Aycan, T. Synthesis, Crystal Structure, Spectroscopic (FT-IR, UV–Vis, EPR) and Hirshfeld Surface Analysis Studies of Zn(II)-Benzoate Coordination Dimer. *J. Mol. Struct.* **2021**, *1223*, 128943-128955.
97. Barra, C.V.; Rocha, F.V.; Netto, A.V.G.; Shimura, B.; Frem, R.C.G.; Mauro, A.E.; Carlos, I.Z.; Ananias, S.R.; Quilles, M.B. New Palladium(II) Complexes with Pyrazole Ligands: Part I. Synthesis, Spectral and Thermal Studies, and Antitumor Evaluation. *J. Therm. Anal. Calorim.*. **2011**, *106*, 483–488.
98. Allan, J.R.; Bonner, J.G.; Bowley, H.J.; Gerrard, D.L.; Hoey, S. Thermal Studies on Fumaric Acid and Crotonic Acid Compounds of Cobalt(II) and Nickel(II). *Thermochim. Acta* **1989**, *141*, 227–233.
99. Sarma, P.; Sharma, P.; Frontera, A.; Barcelo-Oliver, M.; Verma, A.K.; Barthakur, T.; Bhattacharyya, M.K. Unconventional π-Hole and Semi-Coordination Regium Bonding Interactions Directed Supramolecular Assemblies in Pyridinedicarboxylato Bridged Polymeric Cu(II) Compounds: Antiproliferative Evaluation and Theoretical Studies. *Inorganica Chim. Acta* **2021**, *525*, 12046-12060.